TASK QUARTERLY 9 No 2, 245–256

NUMERICAL ANALYSIS OF INTERNAL FLOW PHENOMENA IN A MULTI-BLADE CENTRIFUGAL FAN*

JIABING WANG, YINGDA OU AND KEQI WU

School of Energy and Power Engineering,
Huazhong University of Science and Technology,
Wuhan, Hubei, 430074, P. R. China
hustwjb@163.com

(Received 1 February 2005; revised manuscript received 2 March 2005)

Abstract: A three-dimensional, steady, incompressible, turbulent flow field inside a multi-blade centrifugal fan used in an air-conditioner has been analyzed numerically. Reynolds-averaged Navier-Stokes equations with the standard k-ε turbulence model have been discretized by the finite volume method. The calculation results have shown complex three-dimensional characteristics of the flow, especially in the blade passages near the shroud side. The results have revealed a boundary layer separation at the leading edge on the blade suction surface, the flow reversal from the high pressure region inside the volute to the low pressure region near the impeller inlet, the flow recirculation near the shroud side, a jet-wake pattern at the rotor exit, the pressure fluctuation on the blade surface, *etc.* Some of the numerical results agree well with previous experiment.

Keywords: multi-blade centrifugal fan, internal flow field, CFD

1. Introduction

Multi-blade centrifugal fans have been widely used for air-conditioning systems requiring low noise, small size, relatively high volumetric flow rates, and a high pressure rise. Fans of this type are generally designed to use a large number of forward-curved blades and have a large inlet-exit diameter ratio and a relatively large rotor width, both of which are their key distinguishing features. Thus, the resulting flow inside the fan has complex three-dimensional characteristics.

Earlier researchers have attempted to identify the general flow pattern inside the fan. In the early 1980's, Raj and Swim [1] studied the flow at the exit of a forward-curved (FC) centrifugal fan rotor using the smoke technique and hot wire probes. Their work presented the inactive region at the shroud end of the rotor, the jet-wake velocity profile at the blade exit, and the separated flow at the leading edge of the blade suction surface. Moreover, the flow through the rotor was found to be highly

* The major material has been presented on the 10th International Refrigeration and Air Conditioning Conference at Purdue, USA, 2004.

turbulent and strongly three-dimensional, which was a function of the axial location on the rotor, the tangential position in the housing, and the through flow rate. In the experimental work of Yamazaki and Satoh [2], the main through-flow was near the back plate of the rotor extending for about one fourth of the rotor's width at the inlet and two thirds of its width at the exit, while the remaining rotor span had little through-flow. Later, Kind and Tobin [3] implemented a five-hole probe technique to measure the mean flow field at the rotor inlet and exit, which indicated the presence of a flow reversal through the rotor blade. Thanks to particle tracing velocimetry (PTV), Denger and McBride [4] reported a highly turbulent flow in the vicinity of the volute tongue. Kadota *et al.* [5] and Kawaguchi *et al.* [6] visualized the internal flow field using a spark tracing method and measured the pressure fluctuation on the blade surfaces with a semiconductor-type pressure sensor. They also found a highly complex flow pattern inside the fan and large pressure fluctuation on the blade surfaces near the shroud side of the rotor, as well as passing the volute tongue. Recently, Sandra *et al.* [7] have analyzed the velocity unsteadiness distribution at the impeller outlet with the hot wire technique. They have demonstrated that the unsteady characteristics of the flow are mainly determined by the flow rate and the circumferential position. Basing on these results, many researchers have attempted novel approaches and performed extensive (and partly successful) experiments [8–14] to predict and further improve the fan's performance.

However, most of the research on this type of fans has been experimental. Detailed CFD studies of the internal flow field of integral multi-blade centrifugal fan systems have been relatively limited.

A CFD study can reduce the testing time and the related expense and avoid disturbance of the internal flow field of the fan by the test apartment. Moreover, detailed information on the flow field can be obtained and the flow pattern throughout the fan can be visualized, thus enhancing our understanding of the complex flow physics inside the fan and offering guidance for fan design.

Therefore, the objective of this study is to visualize the main flow phenomena occurring in a multi-blade centrifugal fan, which is extremely difficult using experimental techniques and essential to determine factors influencing the fan's efficiency and noise. This paper presents a numerical simulation of the internal flow field of a multi-blade centrifugal fan used in a household air-conditioner carried out with the FLUENT commercial CFD code. It covers the whole fan system, including the inlet, the impeller and the volute, and presents a detailed analysis on the flow characteristics inside the fan, emphasized by the flow behavior in the blade passage.

2. The fan's configuration

A sketch of the fan used in the present study is shown in Figure 1. The basic geometrical specification and operating conditions are given in Table 1. The fan consists of an inlet section, an impeller of 43 equally spaced straight blades and a volute. It should be noted that the rotor of this fan has been designed as a part with no front plate, but has a very small blade retaining shroud attached to the outer diameter of the blades. However, the shroud has been ignored here for the sake of

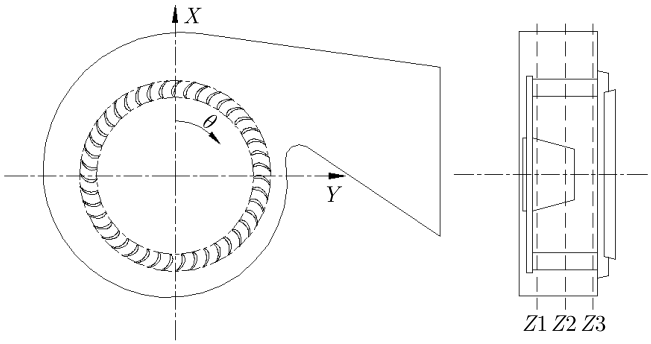

Figure 1. Geometry of the multi-blade centrifugal fan

Table 1. Geometrical specification and operating conditions

Rotor outlet diameter	0.34m	Number of blades	43
Rotor inlet diameter	0.28m	Volute width	0.14m
Rotor width	0.116m	Rotational speed	425rpm
Blade inlet angle	55°	Design flow rate	0.181m^3/s
Blade outlet angle	143°		

computational convenience, so that the flow is fully open on the front side of the impeller.

3. The numerical method

A fully implicit, segregated finite-volume method solving three-dimensional Reynolds-averaged Navier-Stokes viscous partial differential equations has been used in our numerical calculation to study the turbulent flow field of the multi-blade centrifugal fan. The standard two-equation k-ε turbulent model with standard wall functions has been applied to model the turbulent flow. The second-order upwind difference scheme has been employed to spatially discretize the convection terms. The pressure-velocity coupling has been handled using the SIMPLE algorithm.

The flow is assumed to be steady and incompressible. The governing equations of continuity and momentum may be written as:

$$\frac{\partial u_i}{\partial x_i} = 0, \tag{1}$$

$$\frac{\partial}{\partial t}(\rho u_i) + \frac{\partial}{\partial x_j}(\rho u_i u_j) = \rho F_i - \frac{\partial P}{\partial x_i} + \frac{\partial}{\partial x_j}\left(\mu_e\left(\frac{\partial u_i}{\partial x_j} + \frac{\partial u_j}{\partial x_i}\right)\right), \tag{2}$$

where u represents the vector component of three-dimensional Reynolds-averaged velocity, P – the Reynolds-averaged pressure, ρ – density, while F, the body force vector component, represents the Coriolis force and the centrifugal force. μ_e represents turbulent viscosity, given by:

$$\mu_e = \mu + \mu_t, \tag{3}$$

where μ is the coefficient of molecule viscosity and μ_t – the eddy viscosity, estimated from the turbulent kinetic energy, k, and the dissipation rate of turbulent kinetic energy, ε, with the following relationship:

$$\mu_t = \rho C_\mu \left(\frac{k^2}{\varepsilon}\right). \tag{4}$$

k and ε are estimated from semi-empirical transport equations which may be written as follows:

$$\frac{\partial}{\partial t}(\rho k) + \frac{\partial}{\partial x_j}(\rho k u_j) = \frac{\partial}{\partial x_j}\left(\left(\mu + \frac{\mu_t}{\sigma_k}\right)\frac{\partial k}{\partial x_j}\right) + P_k - \rho\varepsilon, \tag{5}$$

$$\frac{\partial}{\partial t}(\rho \varepsilon) + \frac{\partial}{\partial x_j}(\rho \varepsilon u_j) = \frac{\partial}{\partial x_j}\left(\left(\mu + \frac{\mu_t}{\sigma_\varepsilon}\right)\frac{\partial \varepsilon}{\partial x_j}\right) + \frac{C_{1\varepsilon}\varepsilon}{k}P_k - \rho C_{2\varepsilon}\frac{\varepsilon^2}{k}, \tag{6}$$

where P_k is the production of k,

$$P_k = \mu_t\left(\left(\frac{\partial u_i}{\partial x_j}\right) + \left(\frac{\partial u_j}{\partial x_i}\right)\right)\left(\frac{\partial u_i}{\partial x_j}\right). \tag{7}$$

The constants of the above model have the following values:

$$C_\mu = 0.09, \quad C_{1\varepsilon} = 1.44, \quad C_{2\varepsilon} = 1.92, \quad \sigma_k = 1.0, \quad \sigma_\varepsilon = 1.3. \tag{8}$$

4. Grid generation

According to the geometry characteristic of the internal flow field of the multi-blade centrifugal fan, the complex computational domain is subdivided into six regions, which cover the inlet region, the central region, the blade region, the front region, the back region and the volute region. A hybrid structured/unstructured grid of each region is generated independently in order to ensure the grid's quality, save the computer memory and reduce the computational time. The unstructured grid is used on the radial surfaces, as the shape of the internal flow passage along this direction is very irregular, while the structured grid is used in the axial direction. The interface of neighboring sub-regions consists of identical grid nodes. Figure 2 shows the grid of the blade region, which is the main region of energy transference. Compared to the

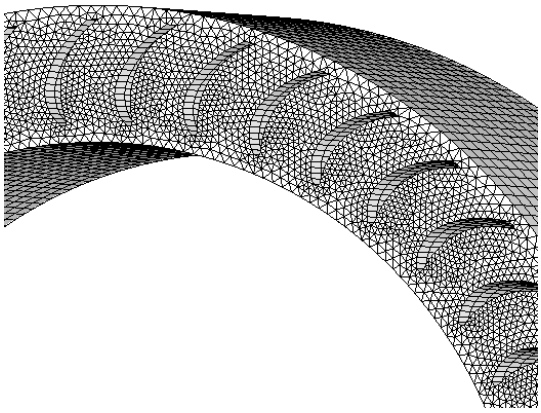

Figure 2. Computational grid of the blade region

other regions, it has a higher grid density (roughly half the total grid number), due to steep gradients of the flow properties. For the same reason, more grid points are focused on the area near the volute tongue in the volute region.

5. Boundary conditions

The inlet of the computational domain is defined as inlet pressure boundary conditions, with specified total pressure, turbulence intensity and hydraulic diameter. In the current simulation, the atmosphere has been set as the inlet boundary conditions. The outlet of the computational domain is defined as outlet pressure boundary conditions, with specified static pressure, backflow turbulence intensity and backflow hydraulic diameter. The impeller's wall is defined as a moving wall with a rotating frame of reference, while other walls are defined as stationary walls in an inertial frame of reference. A no-slip boundary condition is used on the solid walls.

6. Results and discussion

The convergence criterion is set to be 10^{-4} for the residual numbers. The measured static pressure rise for the design flow rate is 36.8Pa, while the calculated value is 38.2Pa. The difference between these is less than 4%, which is within the acceptable range and can validate the numerical results. The flow characteristic yielded by the presented simulation results is discussed in the following subsections. It should be noted that the distributions given below are for the design flow rate, except where specifically stated otherwise.

6.1. The pressure and velocity distribution in particular sections

Figure 3 shows stream lines and velocity vectors (projected onto the X-Z plane) in the $Y = 0$ plane. The flow is sucked into the fan along the axial direction and then gradually turns into a flow along the radial direction near the back plate of the rotor. Thus, the resulting separated flow occurs near the shroud side. Moreover, there is a distinct inactive flow region behind the fan's inlet, as the inlet section is inserted into the top plate of the volute. Therefore, in the absence of the front plate, a flow recirculation region emerges by incorporating the separated and inactive flows, which will lead to a non-uniform outflow at the rotor's exit. Our calculations have shown that the flow recirculation can be expressed as a function of circumferential location. Another notable feature is a small part of the flux entering the impeller from the front side of the rotor, though most of the flux enters the impeller from the rotor's leading edge, which is due to the inlet's outlet diameter being designed larger than the rotor inlet diameter. It is also related with the circumferential location. Additionally,

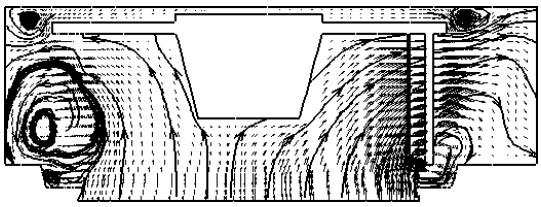

Figure 3. Stream lines and velocity vectors (projected onto the X-Z plane) in the $Y = 0$ plane

Table 2. The flux proportion for various exit static pressures

Fan exit static pressure [Pa]	Q_1 [%]	Q_2 [%]	Q_3 [%]
0	80.7	21.0	1.7
20	81.3	20.5	1.8
30	81.6	20.6	2.2
36	82.1	20.3	2.4
38	82.4	20.2	2.6
39	82.7	20.1	2.8
40	83.1	20.0	3.1

leakage flow occurs through the gap between the rotating wheel and the fan's inlet after the volute tongue, inevitably causing mixing losses inside the fan.

Table 2 lists the flux proportion for various fan exit static pressures. Here, Q_1 represents the proportion of the flux entering the impeller from the rotor's leading edge, Q_2 – the proportion of the flux entering the impeller from the shroud side, Q_3 – the proportion of the flow recirculated behind the fan inlet. Unfortunately, the data shows that the Q_2 percentage is about 20%. Obviously, this part of the flow will have relatively low energy and a negative influence on the fan's performance. It decreases slightly as the fan's exit static pressure is increased, as the flow meets an obstacle in the radial direction. The flow recirculation percentage increases with the fan's exit static pressure, ranging from 1.7 to 3.1, which indicates a great loss for high exit static pressures.

The pressure distribution in the $Z2$ plane, located in the mid plane of the impeller, is illustrated in Figure 4. Clearly, the total pressure distribution is similar to the dynamic pressure distribution due to the forwardcurved blade. Moreover, a considerable pressure difference with the flow of the blade passage is noticeable along the circumferential direction. The main flow region, *i.e.* the blade passages nearest to the volute's exit, has the lowest static pressure and the highest dynamic pressure, as well as the highest total pressure.

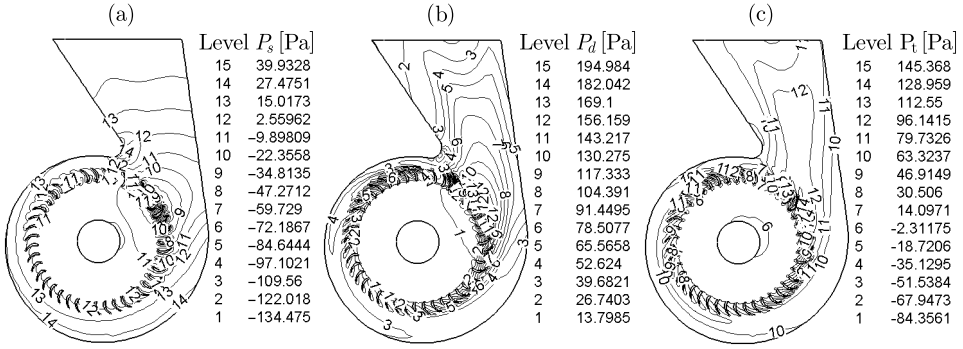

Figure 4. Pressure field in the $Z2$ plane in the middle of the impeller: (a) static pressure; (b) dynamic pressure; (c) total pressure

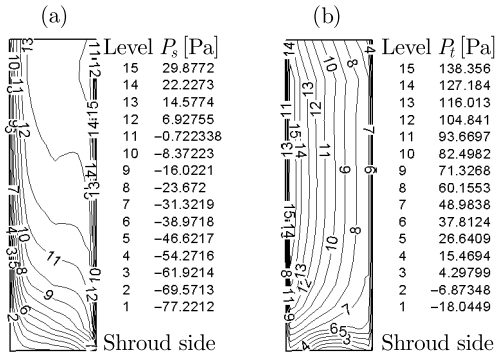

Figure 5. Pressure field in the pressure surface of a blade in the $\theta = 35^{\circ}$ position: (a) static pressure; (b) total pressure

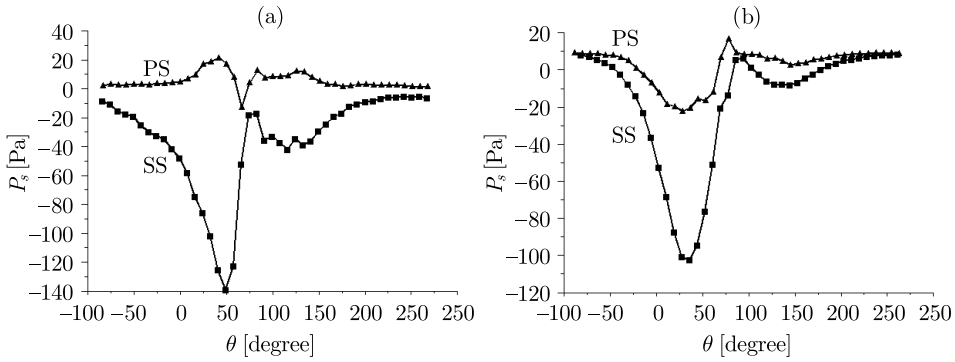

Figure 6. Circumferential distribution of static pressure on the blade surface along the intersecting curve of the $Z2$ plane and the cylindrical plane of the rotor's inlet or outlet (PS – pressure surface, SS – suction surface): (a) inlet; (b) outlet

6.2. The pressure distribution at the blade surfaces

Figure 5 shows a pressure contour diagram in the pressure surface of a blade in the position of $\theta = 35^{\circ}$. Static pressure gradually increases with the flow towards the back plate, while the total pressure increases with the rotor radius due to the wheel's rotation. It should be noted that the flow recirculation causes a large static pressure variation near the shroud side, as well as a large total loss. Along the circumferential direction, the blade surface suffers great pressure fluctuation when it rotates to the main flow region or passes the volute tongue, especially on the suction surface, as shown in Figure 6.

6.3. The vortex flow in the blade passage

Figures 7 and 8 show the stream lines of the blade passages at various axial and circumferential positions. Compared to the blade passages near the back plate, the vortex flow near the shroud side is more pronounced. It occurs in almost all of the blade passages near the shroud side and in about two thirds of the blade passages near the back plate. This is because the flow near the shroud side is basically axial, so it has a small radial velocity, leading to a small blade inlet angle, β_1, and a large attack angle. However, for the flow near the back plate, the change from axial to radial has already been accomplished. Thus the radial velocity is large, which induces a large

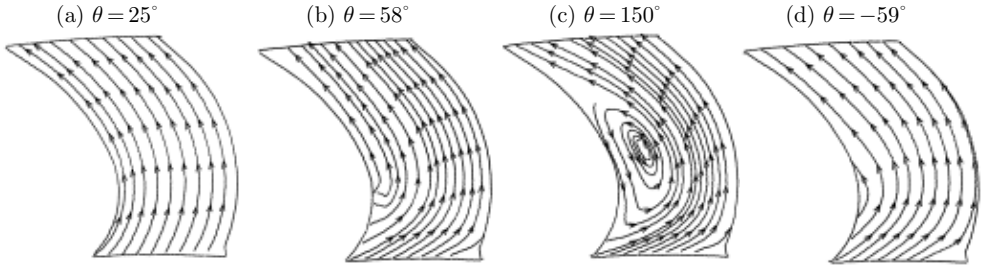

Figure 7. The stream lines at the blade passage near the rotor's back plate in the $Z3$ plane

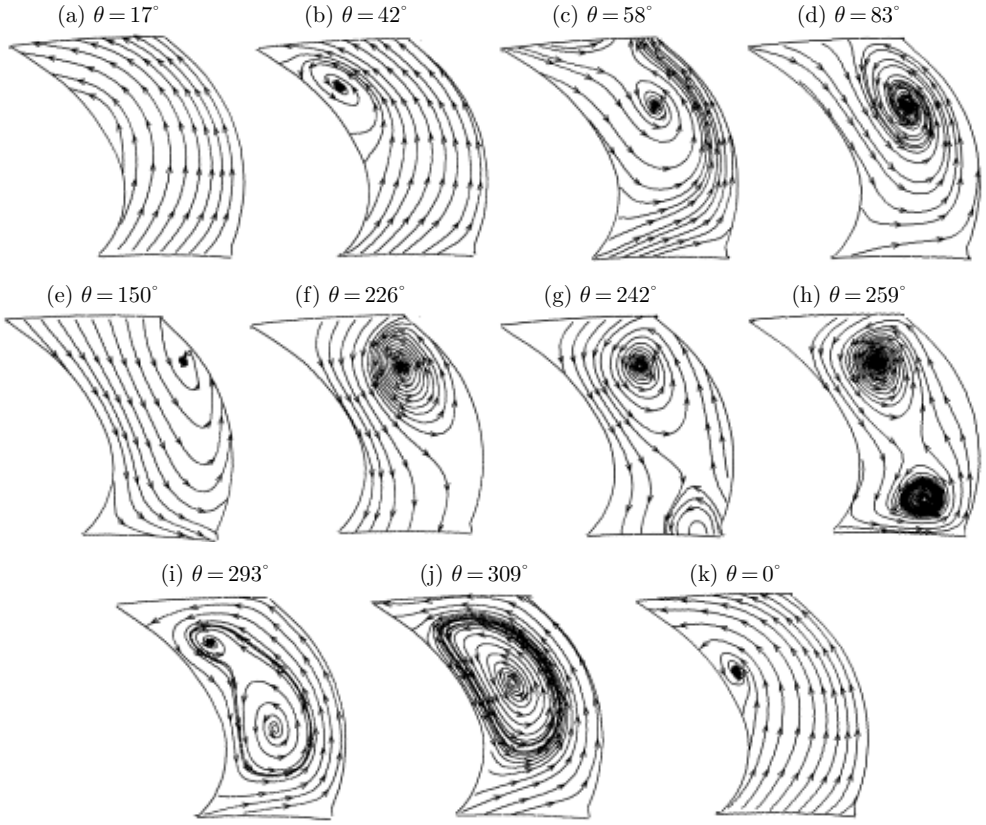

Figure 8. The stream lines at the blade passage near the rotor's shroud side in the $Z1$ plane

blade inlet angle, β_1, and a small attack angle. The greater attack angle makes vortex flow more easily. Even at the same axial location, the attack angle varies along the circumferential direction. The airflow always tends to pass through the rotor from the main flow region, thus leading to a large radial velocity and a small attack angle in these blade passages. Therefore, the area of vortex flow in the main flow region is obviously reduced compared to the blade passages opposite to it. Figure 7a illustrates the flow behavior in the main flow region near the back plate ($-59^{\circ} < \theta < 58^{\circ}$), where the airflow is along the blade surface. Separated flow is generated in the blade passage under the volute tongue (Figure 7b) and increases with the increase of the azimuth angle. The flow is separated at the leading edge of the blade suction surface, and then

reattaches to the blade surface at the trailing edge, as shown in Figure 7c. There is a little outflow near the pressure surface when θ increases to 217°, for a majority of the passage area is filled with the separated flow. Thereafter, radial velocity increases, so that the separated flow decays and finally disappears (Figure 7d). Compared to the blade passages near the back plate, the flow behavior is more complex near the shroud side. Even in the blade passages nearest to the fan's exit, there is a slight separated flow near the blade suction surface due to the small radial velocity and the relatively large tangential velocity (Figure 8a). Along the rotation direction, a vortex is generated near the trailing edge of the suction surface, then gradually increases and moves onto the pressure surface. Simultaneously, a flow reversal from the volute to the blade passage occurs near the suction surface (Figures 8b and 8c). The flow is nearly stagnated in the blade passages under the volute tongue, where there is a region of the largest vortex, as shown in Figure 8d. Then, the vortex continues its movement towards the pressure surface, with its area decreased and the flow reversal developed further. The flow reversal has the strongest influence at $\theta = 150^\circ$, where the reversing flow arrives at the rotor's inlet (Figure 8e). Thereafter, the flow reversal is weakened, the vortex reappears and moves back to the suction surface. Simultaneously, the flow creates a vortex at the leading edge of the pressure surface. While the blade passage continues to move towards the fan's exit, the vortex at the leading edge gradually increases and moves onto the trailing edge of the suction surface, coalesces with the vortex at the trailing edge, decays and finally disappears (Figures 8e–8k). Certainly, the substantial vortex flow is due to the short chord, large width and large curvature of the rotor. Their presence should be for the cause of the poor efficiency and noisiness of the fan.

A similar flow characteristic can be inferred from Figure 9. Clearly, there is a significant difference between the β_1 near the shroud side and that in the middle of the impeller along the circumferential direction. β_1 has negative values in the range of $100^\circ \leq \theta \leq 260^\circ$ near the shroud side, which indicates that the reversed flow occupies up about forty percent of the circumference. Small β_1 ($< 55^\circ$) in the remaining range suggests the occurrence of the separated flow phenomenon. In the middle of the impeller, β_1 has a positive value at each circumferential position, so that no flow reversal occurs there, but separated flow still exists in the blade passages outside the main flow region and, even more so, in the blade passage under the volute tongue.

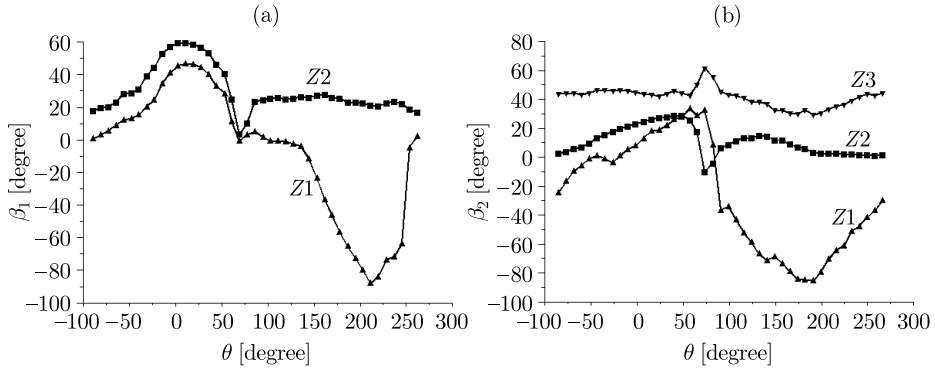

Figure 9. Circumferential distribution of the relative flow angle at the rotor's (a) inlet; (b) outlet

The distribution near the back plate is similar to that in the middle of the impeller (not plotted in this figure). β_2 with negative values occupies up to about two thirds of the circumference near the shroud side, but changes to positive values and evens out towards the back plate.

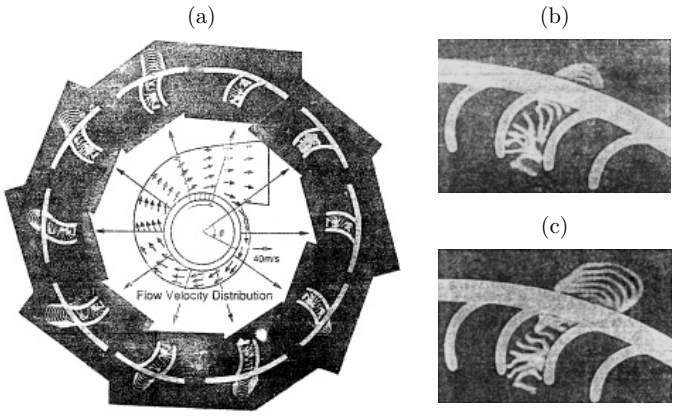

Figure 10. Flow visualization in the blade passage at various axial and circumferential locations: (a) circumferential distribution (reproduced from [5]); (b) near the middle of rotor; (c) near the rotor's back plate (both reproduced from [6])

The above analysis suggests that the flow behavior is different at different axial and circumferential locations. The flow is more easily separable near the front part of the rotor than near its back part. The flow is nearly stagnated in the blade passage under the volute tongue near the rotor's front part, after which a flow reversal occurs. These calculated flow characteristics are in agreement with experimental results found in some of the above-mentioned references. The experimental results obtained with use of the spark tracing method in references [5] and [6] are shown in Figure 10. Figure 10a indicates that the flow of blade passage deteriorates in the vicinity of the volute tongue, while Figures 10b and 10c show that the separated flow is more notable near the middle of the rotor than near the back plate. Moreover, the stagnated flow which occurred near the tongue is in accordance with the results of Denger and McBride [4], who pointed out that those blade passages were full of stalled flow and whose measurement results indicated a minimal through flow.

6.4. The jet-wake velocity profile at the rotor's exit

Figure 11 presents the radial velocity at the rotor's exit in the middle of the impeller. The jet-wake velocity profile is clearly visible, except for the circumferential area closer to the volute tongue where this flow behavior cannot be easily identified due to the interaction with the outflow and the tongue. It is strong in the main flow region ($-15^\circ \leq \theta \leq 15^\circ$) and weak in the region opposite to it, due to the high pressure inside the volute. Moreover, it follows that the jet flow is near the pressure surface and the wake flow is near the suction surface in the region after the volute tongue. But for the main flow region, the high energy flow moves towards the suction surface due to the large radial velocity.

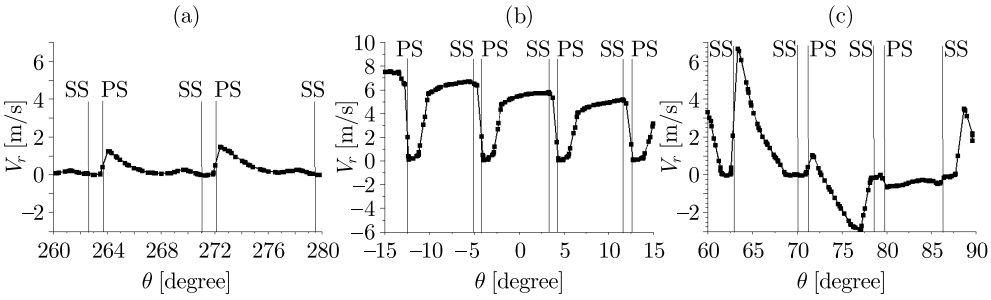

Figure 11. The radial velocity component at the rotor's exit in the $Z2$ plane for different ranges of θ (PS – pressure surface, SS – suction surface)

7. Conclusion

Our three-dimensional numerical analysis of the viscous turbulent flow field in a multi-blade centrifugal fan has been implemented successfully. The calculated flow field distribution provides a comprehensive understanding of the overall flow pattern inside the fan. Some of the numerical results agree well with the earlier experimental results, which indicates the feasibility of the computational model and the numerical method used in the simulation.

There are evident strong three-dimensional characteristics inside the fan when this special geometric configuration is involved. The flow turns from axial to radial after entering the fan. Then, flow recirculation occurs in the region near the shroud side, the area of which is a function of its circumferential location and the through flow rate. A relatively large proportion of the flux is involved in this region for high static pressures at the fan's exit, *i.e.* for low through flow rates. The flow in the blade passage is more complex, especial near the shroud side. Vortex flow has been found to cover most of the flow passages and of the rotor's width, while flow reversal occurs in the blade passages after the volute tongue near the shroud side. Both phenomena are related with the flow rate.The pressure on the blade surface around the rotor has also been examined. A large pressure fluctuation occurs on the blade surface when a blade rotates into the main flow region or passes the volute tongue. Additionally, it cannot be ignored that the flow entering the impeller from the shroud side accounts for about one fifth of the total flux. This part of the flow has relatively low energy. All of these flow features influence the efficiency and noisiness of the fan. Hopefully, the results presented in this paper will contribute much-need improvements in fan performance.

References

[1] Raj D and Swim W B 1981 *Trans ASME, J. Engng. Power* **103** (4) 393
[2] Yamazaki S and Satoh R 1986 *Trans. JSME* **B52** (484) 3987 (in Japanese)
[3] Kind R J and Tobin M G 1990 *Trans. ASME, J. Turbomach.* **112** (1) 84
[4] Denger G R and McBride M W 1990 *Proc. Fluid Measurement and Instrumentation Forum, ASME*, New York, USA, pp. 49–56
[5] Kadota S, Kawaguchi K, Suzuki M, Matsui K and Kikuyama K 1994 *Trans. JSME* **B60** (570) 452 (in Japanese)
[6] Kawaguchi K, Kadota S, Suzuki M, Matsui K and Kikuyama K 1994 *Trans. JSME* **B60** (570) 458 (in Japanese)

[7] Sandra V S, Rafael B T, Carlos S M and Jose G 2001 *Trans. ASME, J. Fluids Engng.* **123** (6) 265
[8] Yamazaki S and Satoh R 1987 *Trans. JSME* **B53** (485) 108 (in Japanese)
[9] Yamazaki S, Satoh R and Ohkuma Y 1987 *Trans. JSME* **B53** (490) 1730 (in Japanese)
[10] Yamazaki S, Hashimoto K and Fukasaku Y 1996 *Trans. JSME* **B62** (602) 3654 (in Japanese)
[11] Yamazaki S, Hashimoto K and Fukasaku Y 1997 *Trans JSME* **B63** (614) 3325 (in Japanese)
[12] Montazerin N, Damangir A and Mirian S 1998 *Proc. Inst. Mech. Engng., J. Power Energy* **212** 343
[13] Montazerin N, Damangir A and Mirzaie H 2000 *Proc. Inst. Mech. Engng., J. Power Energy* **214** 243
[14] Yamamoto S, Kuratani F and Ogawa T 1999 *Trans. JSME* **B65** (635) 2406 (in Japanese)